Optical and Quantum Electronics (2026) 58:324
https://doi.org/10.1007/s11082-026-08918-w

Coupling-induced localization in linearly coupled waveguides with spatially modulated nonlinearity

Bruno M. Miranda[1,2] · **Ardiley T. Avelar**[1] · **Wesley B. Cardoso**[1]

Received: 8 March 2026 / Accepted: 14 May 2026 / Published online: 1 June 2026

Abstract
We study stationary, spatially localized modes in linearly coupled optical waveguides governed by coupled nonlinear Schrödinger equations with asymmetric defocusing Kerr nonlinearities. A waveguide with spatially inhomogeneous nonlinearity supports self-trapped states, whereas a homogeneous defocusing waveguide cannot localize on its own. We show that linear coupling induces localization in the nonlocalizing guide. Fundamental and excited stationary modes are computed, and their existence, power asymmetry, and stability are analyzed as functions of the coupling strength and nonlinearity. Dynamical simulations reveal stable ground and first excited states, whereas higher-order modes are unstable. These results demonstrate coupling-induced spatial localization in defocusing nonlinear waveguide systems.

Keywords Coupling-induced localization · Coupled nonlinear Schrödinger equations · Defocusing Kerr nonlinearity · Linearly coupled optical waveguides

1 Introduction

Spatially localized states in nonlinear wave systems are a cornerstone of nonlinear science and have been extensively studied in contexts ranging from nonlinear optics and Bose–Einstein condensates to plasmas and fluid dynamics (Akhmediev and Ankiewicz 1997; Pethick and Smith 2008; Kono and Skoric 2010). In optical waveguides, the formation of spatial solitons arises from a balance between diffraction and Kerr nonlinearity, enabling self-trapped propagation modes (Kivshar and Agrawal 2003). In their simplest form, such localized states require a self-focusing nonlinear response or an external guiding potential. Conversely, in the absence of external potentials, waveguides dominated by self-defocusing

✉ Wesley B. Cardoso
wesleybcardoso@ufg.br

[1] Instituto de Física, Universidade Federal de Goiás, Goiânia, Goiás 74690-900, Brazil

[2] Instituto Federal de Goiás, Campus Jataí, Jataí, Goiás 75804-714, Brazil

nonlinearities typically do not support stationary localized modes, as nonlinear repulsion enhances diffraction and promotes delocalization.

Several strategies have been proposed to overcome this limitation. One particularly effective approach relies on spatially engineered nonlinear landscapes, where the nonlinear coefficient varies across the transverse coordinate (Borovkova et al. 2011). It has been demonstrated that nonlinear profiles growing away from the waveguide core can act as effective nonlinear traps, supporting bright localized modes even under repulsive self-interactions (Borovkova et al. 2012; Zeng and Malomed 2012; Tian et al. 2012; Cardoso et al. 2013; Wu et al. 2013; Zhong et al. 2018). These concepts have been explored theoretically in optics and matter waves, revealing a rich phenomenology including fundamental and higher-order localized states, existence thresholds, and nontrivial stability properties (Kartashov et al. 2012; Lobanov et al. 2012; Xie et al. 2014; Kartashov et al. 2014; Driben et al. 2015a, b; Kartashov et al. 2017; Zeng et al. 2017; Zeng and Zeng 2020; Santos et al. 2024; Lee et al. 2026).

Independently, linear coupling between adjacent waveguides or cores introduces an additional mechanism for localization and energy redistribution. Coupled nonlinear waveguide systems are known to support a wide variety of collective phenomena, such as symmetric and antisymmetric modes, spontaneous symmetry breaking, mode switching, and complex instability scenarios (Hacker and Malomed 2021; Santos and Cardoso 2023, 2025; Santos et al. 2025; Cardoso and Santos 2025). Specifically, in tunnel-coupled harmonic-oscillator traps, interaction effects give rise to Josephson oscillations, spontaneous symmetry breaking (SSB), and chaotic regimes, with asymmetric trapping enabling confined modes and bound states in the continuum (Hacker and Malomed 2021). Related studies in linearly coupled Bose–Einstein condensates have demonstrated that a potential acting on a single component can induce population imbalance and SSB in the partner field through Rabi coupling (Santos and Cardoso 2023). These concepts have been further extended to systems with fractional diffraction, where nonlinear interaction and anomalous dispersion significantly modify localization and stability properties, leading to symmetry-broken solitons and oscillatory instabilities (Santos and Cardoso 2025). More recently, spatially inhomogeneous nonlinearities have been shown to induce asymmetric soliton pairs in coupled nonlinear Schrödinger systems, with coupling strength and total power playing a decisive role in symmetry control and stability (Santos et al. 2025). In a dissipative setting, induced localization in self-defocusing media was reported using linearly coupled Lugiato–Lefever equations with localized external pumping, demonstrating that gain–loss mechanisms can transfer localization to an otherwise non-confining component (Cardoso and Santos 2025).

In this context, a fundamental and largely unexplored question is whether linear coupling alone can induce localization in a waveguide that is intrinsically unable to support confined modes. Specifically, it remains unclear how a waveguide with a homogeneous, self-defocusing Kerr nonlinearity behaves when coupled to a partner waveguide that supports localization through an inhomogeneous nonlinear profile. Addressing this problem is essential for understanding coupling-induced localization as a generic mechanism in nonlinear systems. In this work, we investigate such a configuration using a coupled nonlinear Schrödinger framework. Through extensive numerical analysis, we demonstrate that linear coupling can transfer localization to the otherwise non-confining waveguide, giving rise to families of coupled soliton-like guided modes with mode-dependent existence, power redistribution, and stability properties.

2 Theoretical model

We consider the spatial propagation of monochromatic optical beams in a system composed of two parallel, linearly coupled optical waveguides with Kerr-type nonlinear response. The evolution of the slowly varying complex field envelopes, $\psi(z,t)$ and $\phi(z,t)$, associated with each waveguide, is described by the following set of coupled nonlinear Schrödinger (cNLS) equations:

$$i\frac{\partial\psi}{\partial z} = -\frac{1}{2}\frac{\partial^2\psi}{\partial x^2} + g(x)|\psi|^2\psi + \kappa\phi, \tag{1}$$

$$i\frac{\partial\phi}{\partial z} = -\frac{1}{2}\frac{\partial^2\phi}{\partial x^2} + G(x)|\phi|^2\phi + \kappa\psi, \tag{2}$$

Here, z denotes the normalized longitudinal propagation distance along the waveguides, while x is the normalized transverse spatial coordinate, along which diffraction takes place. The Laplacian terms account for paraxial diffraction in each guide, whereas the cubic nonlinear terms represent self-phase modulation arising from the Kerr effect. The function $g(x)$ and $G(x)$ are the spatially dependent nonlinear coefficients, which may differ between the two waveguides, allowing for asymmetric nonlinear responses.

The parameter κ is the constant linear coupling coefficient resulting from evanescent field overlap between the neighboring waveguides. This coupling enables coherent energy exchange between the channels and plays a central role in the formation of composite localized states. In the absence of coupling ($\kappa = 0$), each waveguide evolves independently according to its own nonlinear response.

In this work, we focus on a configuration in which the first waveguide exhibits a spatially inhomogeneous self-defocusing nonlinearity, while the second waveguide is characterized by a homogeneous Kerr response. Specifically, the nonlinear coefficients are chosen as

$$g(x) = \cosh^2(x), \quad G(x) = G, \tag{3}$$

where G is a real constant. The nonlinearity profile $g(x)$ increases away from the transverse center, effectively generating a nonlinear trapping mechanism that supports spatially localized modes despite the defocusing nature of the Kerr response, as previously reported in Refs. (Borovkova et al. 2011, 2012; Zeng and Malomed 2012; Tian et al. 2012; Wu et al. 2013; Cardoso et al. 2013; Zhong et al. 2018). In contrast, the homogeneous waveguide with constant $G > 0$ cannot sustain localized states in isolation. As demonstrated below, linear coupling between the guides induces localization in the second waveguide, giving rise to coupled soliton complexes.

A fundamental conserved quantity of the coupled system is the total power (or optical norm),

$$P_m = \int_{-\infty}^{+\infty} \left(|\psi_m(x,z)|^2 + |\phi_m(x,z)|^2\right) dx, \tag{4}$$

which remains invariant during propagation. The total power acts as a fundamental control parameter determining the existence, stability, and structural properties of stationary localized modes and is systematically used to characterize and organize the associated solution families. The integer index $m = 0, 1, 2, 3$ labels the fundamental state and successive higher-order stationary states.

3 Numerical results

In this section, we present the numerical results obtained from the cNLS equations, Eqs. (1) and (2). Stationary localized solutions corresponding to the fundamental and higher-order (excited) modes are computed using the imaginary-time propagation method (Yang 2010). The numerical implementation is based on a split-step Fourier scheme, in which the linear diffraction operator is treated in the spectral domain, while the nonlinear terms are evaluated in real space using a standard exponential time-stepping algorithm (for more details, see Ref. Cardoso 2025).

To accurately compute higher-order stationary states, a Gram–Schmidt orthogonalization procedure is incorporated into the imaginary-time iterations. Starting from a set of trial functions $\{\bar{\psi}^0, \ldots, \bar{\psi}^k\}$, the method constructs an orthogonal set $\{\psi^0, \ldots, \psi^k\}$ by sequentially removing the projections onto all previously obtained lower-order modes. Specifically, the *j*-th mode is obtained as

$$\psi^j(z) = \bar{\psi}^j(z) - \sum_{n=0}^{j-1} \psi^n(z) \frac{\int_{-\infty}^{+\infty} \bar{\psi}^j(z)\psi^n(z)}{\int_{-\infty}^{+\infty} \psi^n(z)\psi^n(z)}, \tag{5}$$

with the initial condition $\psi^0 = \bar{\psi}^0$, and $j > 0$. An analogous orthogonalization procedure is simultaneously applied to the ϕ component to ensure the self-consistent convergence of the coupled system.

All simulations are performed in a transverse computational window of size $L = 40$, discretized using $N_x = 1024$ grid points. The imaginary-time evolution is carried out with a fixed step size $\Delta\tau = 0.01$ for up to 2×10^4 iterations, which is sufficient to ensure convergence to stationary states. Unless otherwise stated, all solutions are obtained under the normalization condition $P = 1$.

Figure 1 shows an illustrative example of the stationary intensity profiles of the fundamental and higher-order modes ($m = 0, \ldots, 3$) for a family of coupled solitons with parameters $\kappa = 2.0$, $G = 1.8$, and $P = 1$. Solid blue and dashed black curves correspond to the ψ and ϕ components, respectively. Despite the fact that the second waveguide operates in the self-defocusing regime ($G > 0$), the linear coupling κ effectively induces spatial localization in the ϕ field. The interaction with the first waveguide, which supports localized modes due to its spatially inhomogeneous nonlinearity, overcomes the intrinsic repulsive self-interaction of the homogeneous guide and enforces a soliton-like profile in the coupled component.

For $\kappa = 2.0$ and $G = 1.8$, Fig. 1a shows that the two field components exhibit nearly identical transverse profiles in the fundamental state, characterized by comparable peak intensities and spatial widths. In contrast, a pronounced asymmetry between the components

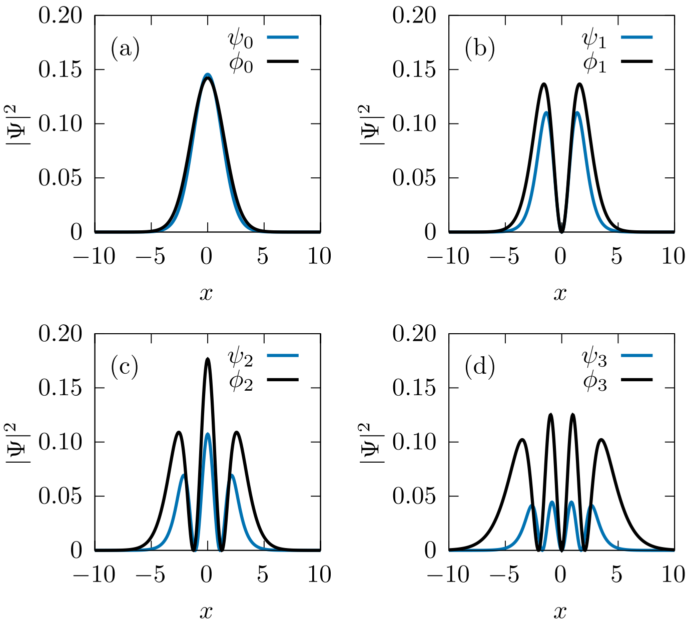

Fig. 1 Stationary transverse intensity profiles of coupled soliton modes in linearly coupled waveguides: **a** fundamental mode ($m = 0$) and **b**–**d** higher-order excited states ($m = 1, 2, 3$). Solid (blue) and dashed (black) curves correspond to the ψ and ϕ field components, respectively. The stationary solutions are obtained using the imaginary-time propagation method applied to Eqs. (1) and (2), for coupling strength $\kappa = 2.0$, homogeneous nonlinearity $G = 1.8$, and total power $P = 1$

emerges for higher-order modes, as shown in Fig. 1b–d. Although both ψ and ϕ display the characteristic multi-lobed structures associated with excited states, the ϕ component consistently develops broader spatial profiles and higher peak intensities than its ψ counterpart.

This behavior originates from the distinct nonlinear responses of the two waveguides. The spatially modulated nonlinearity $g(x) = \cosh^2(x)$ provides an effective nonlinear confinement that increasingly suppresses the transverse expansion of the ψ field as $|x|$ grows. By contrast, the second waveguide, characterized by a homogeneous defocusing nonlinearity ($G > 0$), experiences a repulsive self-action that naturally favors spatial broadening. Under the action of linear coupling, this repulsive tendency does not prevent localization but instead leads to wider soliton profiles with enhanced peak amplitudes in the ϕ component. As a result, the interplay between nonlinear inhomogeneity and linear coupling induces a significant redistribution of energy toward the homogeneous waveguide, allowing the ϕ field to sustain larger amplitudes despite its intrinsically defocusing character.

We next analyze the influence of the system parameters G, κ, and P on the spatial structure of the coupled modes. For clarity, we focus on the first excited state ($m = 1$), noting that the qualitative trends discussed below are representative of all higher-order solutions obtained in our simulations. Figure 2a and b illustrate the evolution of the transverse intensity profiles as the homogeneous nonlinearity strength G is increased, while keeping the coupling fixed at $\kappa = 2.0$. For relatively weak defocusing ($G = 2$, solid curves), the ϕ component exhibits higher peak intensity than the ψ field. However, as the nonlinearity is

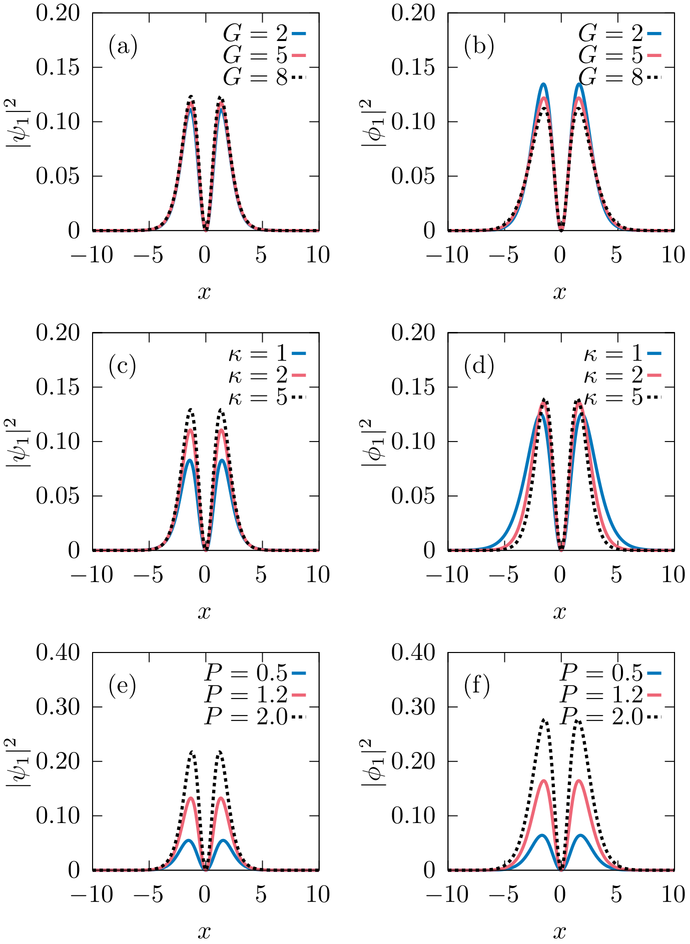

Fig. 2 Stationary transverse intensity profiles of the first excited state ($m = 1$) in linearly coupled waveguides. The left and right columns show the ψ and ϕ field components, respectively. Panels **a** and **b** illustrate the effect of the homogeneous nonlinearity strength G at fixed coupling $\kappa = 2.0$ and total power $P = 1$; panels **c** and **d** show the influence of the linear coupling coefficient κ for fixed $G = 1.8$ and $P = 1$; panels **e** and **f** depict the dependence on the total power P at fixed $\kappa = 2.0$ and $G = 1.8$

increased to $G = 8$ (dotted curves), a clear inversion of the peak intensities occurs, with the ψ component becoming dominant.

Since the total power P is conserved, this inversion is driven by the strengthening of the repulsive self-defocusing interaction in the homogeneous waveguide. As G increases, the enhanced nonlinear repulsion progressively suppresses localization in the ϕ field, forcing a transfer of energy toward the ψ component, which remains efficiently confined by the spatially increasing nonlinear profile $g(x)$. Consequently, increasing G leads to a systematic reduction of the peak intensity in the ϕ component, accompanied by a concurrent enhancement of the ψ field, highlighting the competitive balance between nonlinear repulsion and coupling-induced localization.

We next examine the role of the linear coupling coefficient κ, keeping the homogeneous nonlinearity fixed at $G = 1.8$. The corresponding transverse intensity profiles for different coupling strengths are shown in Fig. 2c and d. As the coupling increases, a clear trend toward a more balanced energy distribution between the two waveguide components is observed. For relatively weak coupling, $\kappa = 1$ (solid blue curves), the ϕ field exhibits a substantially higher peak intensity than the ψ component, indicating that localization in the homogeneous waveguide is only weakly mediated by the interaction with its partner. In contrast, when the coupling strength is increased to $\kappa = 5$ (dotted black curves), the peak amplitude of the ψ soliton rises significantly, reflecting an enhanced bidirectional energy exchange between the guides.

In addition to redistributing power, stronger linear coupling induces a pronounced spatial compression of the ϕ component. This effect arises from the intensified interaction with the ψ field, which is tightly confined by the spatially increasing nonlinear profile $g(x)$. As a result, the effective trapping imposed through coupling overcomes the intrinsic self-defocusing tendency of the homogeneous waveguide, forcing the ϕ field to adopt a narrower and more localized transverse profile. This behavior highlights the central role of linear coupling as an effective mechanism for transferring confinement properties between dissimilar nonlinear media.

Finally, Fig. 2e and f display the stationary profiles obtained by varying the total power P, while keeping $G = 1.8$ and $\kappa = 2.0$, consistent with the configuration shown in Fig. 1. As expected for spatially localized solutions in Kerr-type nonlinear systems, a reduction of the total power to $P = 0.5$ (solid blue curves) leads to a substantial decrease in the peak intensities of both field components. Conversely, increasing the power to $P = 2.0$ (dotted black curves) results in a marked enhancement of the soliton amplitudes. Within the explored parameter range, variations in P primarily rescale the field intensities without altering the qualitative spatial structure of the modes, in agreement with the standard behavior of solitons in linearly coupled nonlinear waveguides.

To further elucidate the role of the homogeneous nonlinearity in the second waveguide, we perform an extensive parametric sweep over the coefficient G. This analysis is aimed at quantifying the dependence of both the peak intensity and the transverse confinement of the coupled soliton modes on the strength of the defocusing nonlinearity. Figure 3a–d display the maximum intensity of the stationary solutions as a function of G, with the linear coupling fixed at $\kappa = 2.0$. In these panels, the vertical axis Ψ_m denotes the peak amplitude of the stationary mode corresponding to the order m.

Consistent with the trends observed in Fig. 2, the results reveal a pronounced crossover in the peak intensities of the two field components as G increases. For weak defocusing (G small), the ϕ component (dashed black curves) exhibits higher peak intensities than the ψ field (solid blue curves), indicating that the coupling-induced localization in the homogeneous waveguide is dominant in this regime. However, as the defocusing nonlinearity strengthens, an increasing fraction of the total power is expelled from the ϕ component due to enhanced nonlinear repulsion and is consequently transferred to the ψ field, which remains efficiently confined by the spatially modulated nonlinearity $g(x)$.

As a result, the ψ component eventually attains a larger maximum intensity than the ϕ field, marking a clear transition in the dominant localization channel. This crossover occurs at $G \approx 1.5$ for the fundamental mode ($m = 0$) and shifts to significantly higher values, $G \approx 5.8$, for the first excited state ($m = 1$). A similar qualitative behavior is observed for

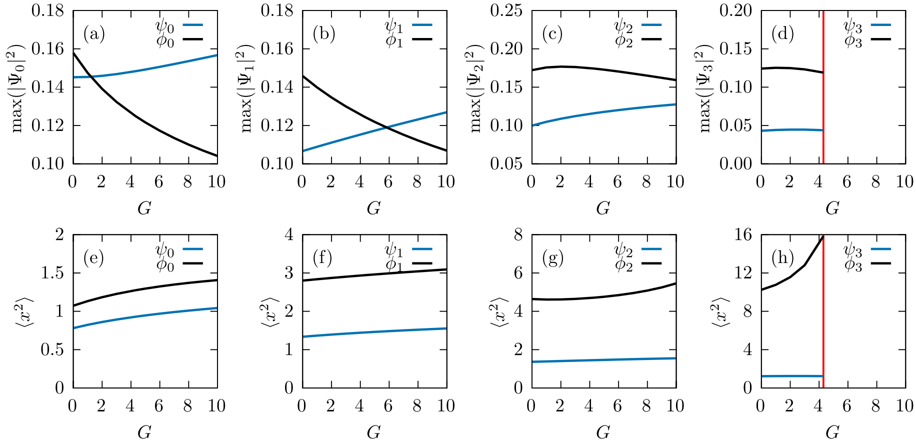

Fig. 3 Dependence of stationary coupled soliton characteristics on the homogeneous nonlinearity strength G for fixed coupling $\kappa = 2.0$ and total power $P = 1$. Top row **a**–**d** shows the peak intensities Ψ_m of the fundamental ($m = 0$) and higher-order modes ($m = 1, 2, 3$) as functions of G. Bottom row **e**–h displays the corresponding root-mean-square (RMS) widths $\langle x^2 \rangle$ versus G. The vertical red dashed lines in panels **d** and **h** mark the delocalization threshold of the third excited mode ($m = 3$)

the second excited mode ($m = 2$), for which the intersection point is expected to occur at values of G exceeding the parameter range explored here. This progressive shift of the crossover with increasing mode order reflects the enhanced spatial extent and reduced confinement efficiency of higher-order modes.

We next examine the root-mean-square (RMS) width, $\langle x^2 \rangle$, which provides a quantitative measure of the transverse spatial extent and degree of localization of the stationary modes. Figure 3e–h present the dependence of $\langle x^2 \rangle$ on the homogeneous nonlinearity strength G for the fundamental and higher-order states, with the coupling fixed at $\kappa = 2.0$. The results demonstrate that increasing G leads to a systematic broadening of all considered modes, reflecting the progressively stronger defocusing contribution of the homogeneous waveguide.

For the ϕ component, this spatial expansion is accompanied by a monotonic reduction of the peak intensity, consistent with the dominant repulsive self-interaction. In contrast, the ψ component exhibits a more subtle behavior: although its RMS width increases with G, the concomitant transfer of power from the ϕ field results in a simultaneous enhancement of the peak intensity. This coexistence of increasing width and amplitude highlights the nontrivial balance between nonlinear confinement induced by the inhomogeneous profile $g(x)$ and the coupling-mediated energy redistribution.

A critical delocalization behavior is observed for the third excited state ($m = 3$), as shown in Fig. 3h. At $G \approx 4.3$ (indicated by the red dashed line), the repulsive self-defocusing interaction in the homogeneous waveguide becomes sufficiently strong that the ϕ component undergoes rapid spatial expansion and effectively reaches the boundaries of the computational domain. This marks the loss of transverse confinement and signals a transition from a genuinely localized mode to an effectively unbounded state. The breakdown of localization at this threshold is further corroborated by the abrupt termination of the corresponding peak-intensity curve in Fig. 3d, indicating the absence of stationary solutions beyond this critical value of G.

The preceding analysis demonstrates that both the nonlinear self-interaction and the linear coupling strength have a profound impact on the spatial structure and energetic properties of the stationary modes, including the partition of power between the two coupled waveguides. To quantify this redistribution, we introduce the power asymmetry parameter η, defined as

$$\eta = \frac{P_\psi - P_\phi}{P_\psi + P_\phi}, \tag{6}$$

which provides a normalized measure of the relative power imbalance between the two field components. The dependence of η on the homogeneous nonlinearity coefficient G is shown in Fig. 4a–d for different values of the linear coupling strength κ. Since the total power is fixed at $P = 1$, the parameter η directly reflects the redistribution of energy between the waveguides.

As illustrated in Fig. 4a, the higher-order modes $m = 2$ and $m = 3$ exist at weak coupling ($\kappa = 1.0$) only when the second waveguide operates in the self-focusing regime ($G < 0$). In this parameter region, the attractive nonlinearity of the ϕ component compensates for the insufficient linear coupling, thereby enabling the localization of these excited states. Over most of the investigated parameter range, the power carried by the ϕ field exceeds that of the ψ component, resulting in negative values of the asymmetry parameter ($\eta < 0$). This imbalance becomes increasingly pronounced for higher-order modes, reflecting their larger spatial extent and stronger sensitivity to coupling-induced localization.

Importantly, the magnitude of the asymmetry decreases systematically as the coupling strength κ is increased. Stronger linear coupling enhances bidirectional energy exchange between the waveguides and promotes a more symmetric power distribution, driving η toward zero. This behavior corroborates and extends the trends observed in Fig. 2, confirming that linear coupling acts as an efficient control parameter for balancing energy between dissimilar nonlinear waveguides and mitigating the intrinsic asymmetry imposed by their distinct nonlinear responses.

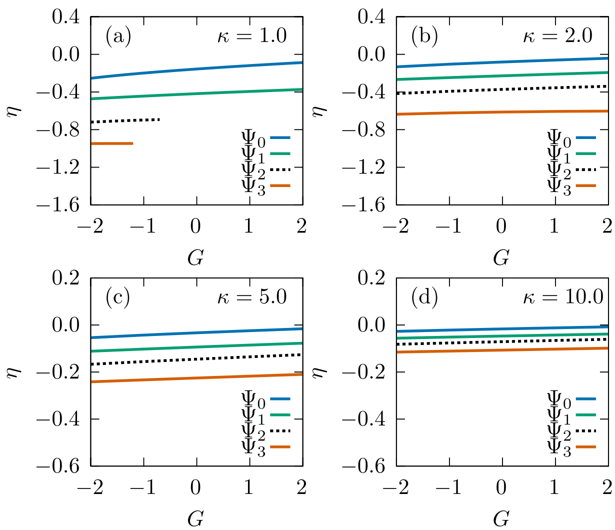

Fig. 4 Power asymmetry parameter η as a function of the homogeneous nonlinearity coefficient G for different linear coupling strengths: **a** $\kappa = 1.0$, **b** $\kappa = 2.0$, **c** $\kappa = 5.0$, and **d** $\kappa = 10.0$, with the total power fixed at $P = 1$. Solid blue, dashed green, dotted black, and dash-dotted orange curves correspond to the fundamental mode ($m = 0$) and the first, second, and third excited states ($m = 1, 2, 3$)

To further elucidate the mechanisms governing power redistribution between the coupled fields, we analyze the dependence of the asymmetry parameter η on the linear coupling strength κ for fixed values of the homogeneous nonlinearity coefficient G. The corresponding results are presented in Fig. 5a–d for $G = -1.0$, 1.0, 5.0, and 10.0, respectively. This analysis complements and extends the results discussed above by explicitly demonstrating the role of linear coupling as a control parameter for energy sharing between the two waveguides.

Across all considered values of G, the numerical results show that increasing κ systematically drives the system toward a more symmetric power distribution, with the asymmetry parameter η approaching zero in the strong-coupling limit. This behavior reflects the enhanced efficiency of bidirectional energy exchange between the waveguides as the coupling strength increases, progressively suppressing the imbalance imposed by their distinct nonlinear responses.

A notable feature of these curves is the abrupt onset of the solution branches for each mode, which signals the existence of a minimum coupling threshold required for the formation of stationary localized states under the chosen parameter conditions. Below this threshold, the linear interaction between the waveguides is insufficient to compensate for diffraction and nonlinear repulsion, preventing the stabilization of localized solutions. The position of this threshold depends on both the nonlinearity strength G and the mode order, underscoring the intricate interplay between coupling, nonlinearity, and modal structure in the formation of coupling-induced solitons.

A key physical insight arises from the comparison between local peak intensities and the global power distribution. Although large values of the homogeneous nonlinearity G induce a crossover in the peak amplitudes of the two components, as demonstrated in Fig. 3, the asymmetry parameter η associated with higher-order modes remains strictly negative throughout the explored coupling range. This behavior indicates that, despite the effective suppression of the maximum amplitude of the ϕ component by strong self-defocusing, its substantially broader spatial extent, quantified by the increased RMS width $\langle x^2 \rangle$ in Fig. 3, allows it to retain a dominant fraction of the total power. In contrast, for the fundamen-

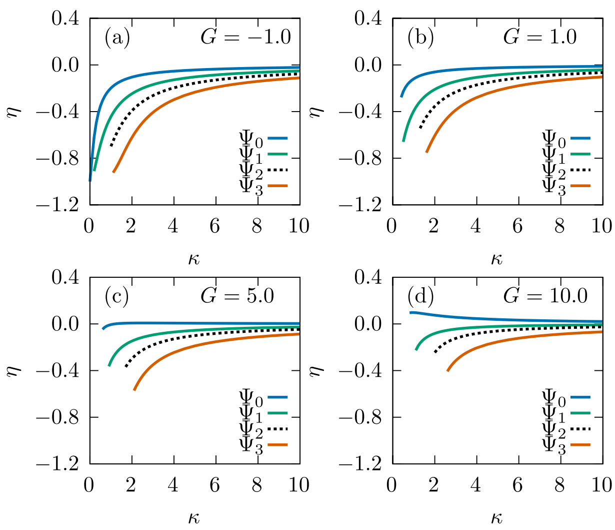

Fig. 5 Power asymmetry parameter η as a function of the linear coupling strength κ for fixed homogeneous nonlinearity coefficients: **a**$G = -1.0$, **b**$G = 1.0$, **c**$G = 5.0$, and **d**$G = 10.0$, with the total power set to $P = 1$. Solid blue, dashed green, dotted black, and dash-dotted orange curves correspond to the fundamental mode ($m = 0$) and the first, second, and third excited states ($m = 1, 2, 3$), respectively

tal mode under strong repulsive conditions (Fig. 5d, $G = 10.0$), the asymmetry parameter crosses zero and becomes positive, revealing that in this regime the self-defocusing nonlinearity of the ϕ field is sufficiently strong to reverse both the local peak intensity hierarchy and the global power balance between the two components.

To obtain a comprehensive picture of the system's parameter space, we carried out a systematic two-dimensional scan over the self-defocusing strength G and the linear coupling coefficient κ. For each point in the (G, κ) plane, the maximum peak intensity $\max|\Psi_m|^2$ was computed with a resolution of 0.1. The resulting maps, shown in Fig. 6a–h, simultane-

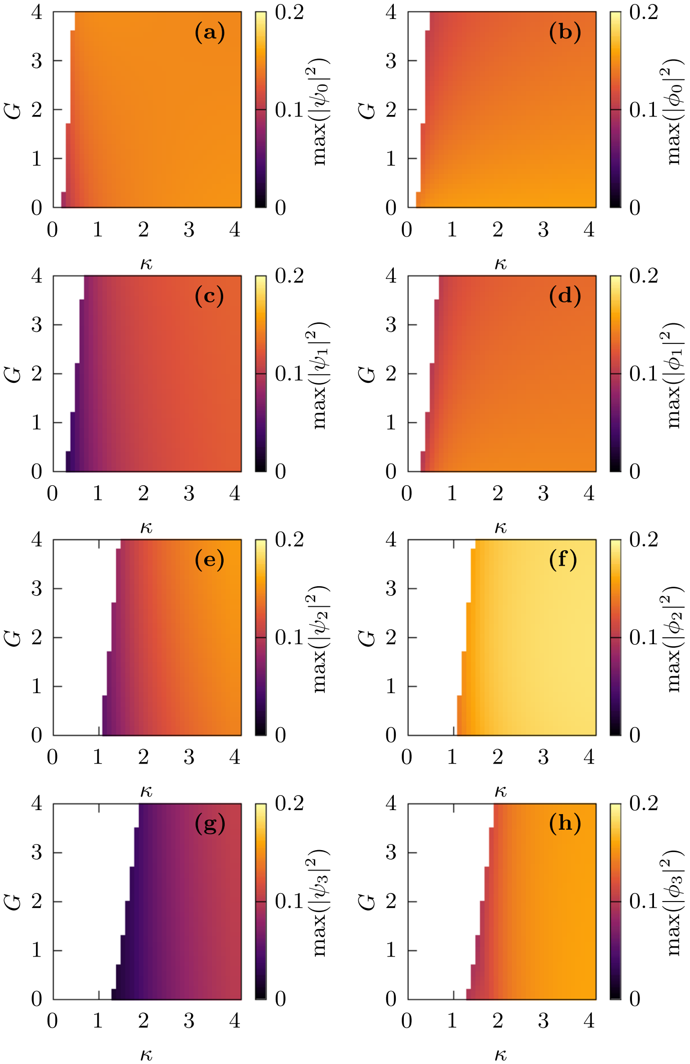

Fig. 6 Peak-intensity maps $\max|\psi_m|^2$ (left) and $\max|\phi_m|^2$ (right) in the (κ, G) plane for stationary modes $m = 0, 1, 2, 3$ at $P = 1$ ($\kappa \geq 0.1$). White regions indicate the absence of localized solutions. The color scale represents the maximum field amplitude and illustrates the redistribution of intensity between the coupled components

ously provide existence diagrams for stationary localized modes and intensity heatmaps, where the color scale encodes the peak amplitudes of the ψ and ϕ components for each mode m. These diagrams allow for a direct visualization of the interplay between coupling and nonlinearity in determining both the localization properties and the inter-component power distribution of the system.

A salient feature of the maps in Fig. 6 is the presence of extended white regions, which delineate parameter domains where the system fails to sustain stationary localized solutions. Importantly, the location of these existence boundaries exhibits a pronounced dependence on the mode index m. Whereas the fundamental mode ($m = 0$) persists over almost the entire explored parameter space, higher-order modes require progressively stronger linear coupling κ to counterbalance the increasing influence of the self-defocusing nonlinearity G. As a result, the existence boundaries systematically shift toward larger κ values as the mode order increases from $m = 0$ to $m = 3$. This trend indicates that excited states are intrinsically more sensitive to the competition between linear coupling and nonlinear repulsion, demanding a stronger inter-core interaction to preserve their multi-nodal structure against delocalization.

The phase diagrams in Fig. 6 further substantiate and extend the preceding analysis. In particular, the intensity maps of the ϕ-field component (right column) exhibit systematically lighter color tones compared to their ψ-field counterparts (left column), indicating larger peak amplitudes in the second field. This contrast reveals a pronounced intensity and power imbalance in favor of the ϕ component in the weak-coupling regime. The effect becomes increasingly pronounced for higher-order modes, where the strong color contrast between panels (g) and (h) highlights the combined action of the effective confinement imposed by the inhomogeneous nonlinearity profile $g(x)$ and the homogeneous self-defocusing nonlinearity G, which together promote energy accumulation in the partner waveguide.

Figure 7 summarizes the existence boundaries of the higher-order modes $m = 2$ and $m = 3$ for different total power levels. The numerical results show that reducing the total power ($P < 1$) shifts the existence regions toward lower coupling strengths, effectively expanding the domain of localized solutions. Physically, this behavior arises because a smaller norm weakens the effective nonlinear self-repulsion, allowing the linear coupling κ to sustain localization even at reduced values. In this low-power regime, the existence

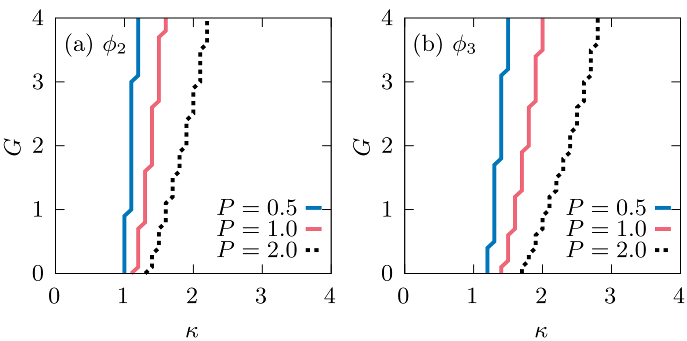

Fig. 7 Existence boundaries of stationary localized solutions for the higher-order modes **a** $m = 2$ and **b** $m = 3$ at different total power levels. Solid blue, dashed red, and dotted black curves correspond to $P = 0.5$, $P = 1.0$, and $P = 2.0$, respectively. Localized stationary modes exist only in the parameter regions to the right of each boundary

boundaries become nearly vertical, indicating a diminished sensitivity of the localization threshold to variations in G for fixed κ.

Conversely, increasing the total power ($P > 1$) raises the effective energy barrier for the formation of stationary localized states, thereby shifting the existence boundaries toward larger values of the coupling coefficient κ. In this high-power regime, the competition between nonlinear self-repulsion and linear coupling becomes increasingly severe, requiring substantially stronger inter-core coupling to prevent mode delocalization. The corresponding transition curves acquire a steeper, diagonally oriented profile, indicating that at elevated power levels the structural integrity of the solitons depends sensitively on a fine balance between coupling strength and nonlinear intensity. A direct comparison between Fig. 7a and b further reveals that the existence threshold for the $m = 3$ mode is systematically shifted to higher κ values than for $m = 2$, confirming that increasing nodal complexity significantly hinders the formation and persistence of localized states.

A central component of the present study is the assessment of the dynamical stability of the stationary modes supported by the coupled system. To this end, the stationary solutions were propagated in real time after introducing a 4% random perturbation to their initial amplitudes. The time evolution was performed using the split-step Fourier method with a z-coordinate step size $\Delta z = 10^{-4}$, and extended up to a final propagation position $z = 2 \times 10^4$ in order to capture long-term dynamical behavior.

Figure 8a–h display representative real-time evolution results for the parameter set $\kappa = 2.0$, $G = 1.8$, and $P = 1$, showing the intensity dynamics of the ψ_m (top row) and ϕ_m (bottom row) components. The simulations demonstrate that both the fundamental ($m = 0$) and the first excited ($m = 1$) modes remain dynamically robust against the imposed perturbations, preserving their spatial profiles and peak intensities throughout the entire propagation. Notably, the evolution of the two coupled components remains fully synchronized, indicating strong mutual locking induced by the linear coupling.

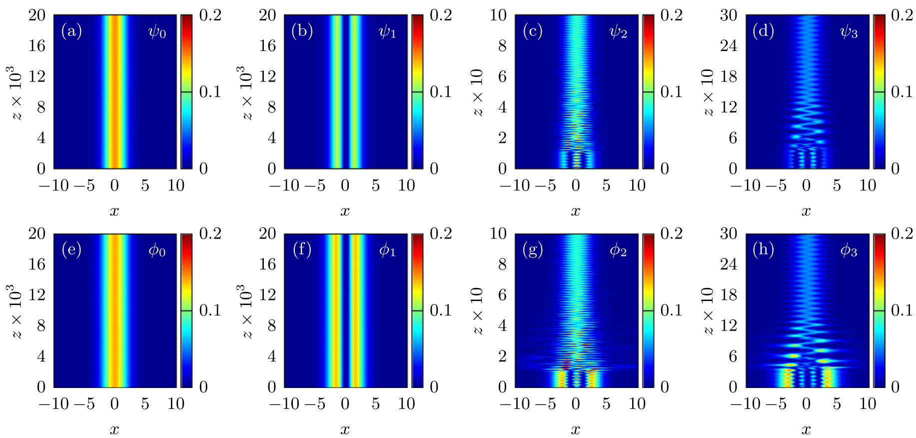

Fig. 8 Real-time evolution of the intensities $|\psi_m|^2$ (top) and $|\phi_m|^2$ (bottom) for the coupled modes $m = 0, 1, 2,$ and 3 by considering the parameter values $\kappa = 2.0$, $G = 1.8$, and total power $P = 1$. Panels **a**–**d** correspond to increasing mode order. Dynamical stability is probed by introducing a 4% random perturbation to the initial stationary profiles at $z = 0$. The long-distance preservation of the field structure confirms the robustness of the fundamental and first excited states ($m = 0, 1$), whereas higher-order modes exhibit pronounced instability under identical conditions

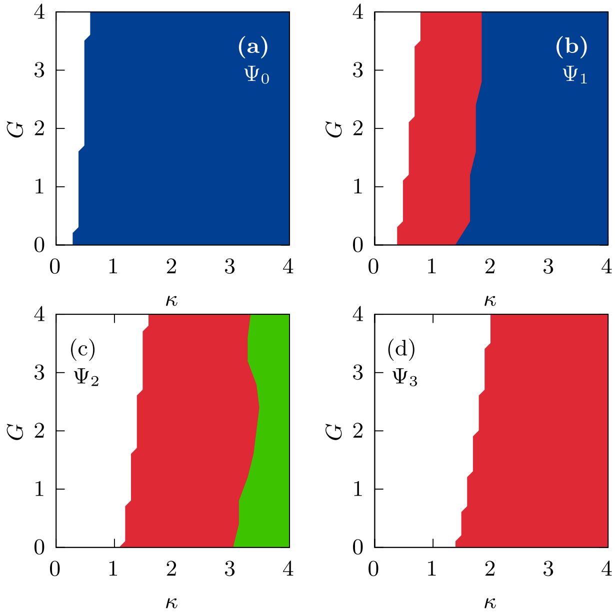

Fig. 9 Stability phase diagrams in the (κ, G) parameter space for guided modes with indices **a**$m = 0$, **b**$m = 1$, **c**$m = 2$, and **d**$m = 3$, at fixed total power $P = 1$ ($\kappa \geq 0.1$). Blue regions correspond to dynamically stable propagation of stationary localized modes. Red regions indicate oscillatory or decay instabilities resulting in relaxation toward the fundamental mode ($m = 0$). The green region in panel (c) denotes unstable evolution with decay into the first excited state ($m = 1$). White areas mark parameter domains where stationary localized solutions are not supported

In contrast, the higher-order guided modes ($m = 2$ and $m = 3$) exhibit a markedly enhanced sensitivity to perturbations, rapidly evolving into oscillatory instability regimes followed by pronounced structural breakup. This dynamical evolution is accompanied by the emission of dispersive radiation into the transverse continuum and a progressive loss of modal coherence, ultimately leading to relaxation toward lower-order guided states, predominantly the fundamental mode. Notably, this decay process occurs in a correlated manner across both coupled waveguides, indicating that the linear coupling enforces a collective instability mechanism that is largely insensitive to the initial disparity in peak intensities between the two field components. These observations demonstrate that the increased nodal complexity of higher-order guided modes substantially reduces their robustness against external perturbations, rendering multi-lobed stationary profiles intrinsically unstable even for moderate inter-waveguide coupling strengths.

To complete the analysis, we performed a systematic numerical stability survey by propagating the stationary solutions in real time across the (G, κ) parameter space. Based on these simulations, stability phase diagrams were constructed to delineate the domains of dynamically stable and unstable propagation. Figure 9a–d present the resulting stability maps for the fundamental mode ($m = 0$) and the excited guided modes ($m = 1, 2,$ and 3), respectively, with the total power fixed at $P = 1$. These diagrams provide a comprehensive classification of the dynamical response of the coupled waveguide system, highlighting the parameter regimes in which linear coupling can effectively counteract nonlinear self-repulsion to stabilize localized guided modes.

For the fundamental guided mode, Fig. 9a, the stationary solutions exhibit robust dynamical stability throughout their entire existence domain. Even in the presence of random initial perturbations, the $m = 0$ mode preserves its transverse intensity profile and phase coherence during propagation, confirming its role as the global ground state of the coupled waveguide system. This behavior reflects the fact that the fundamental mode corresponds to the lowest-energy configuration and is therefore resilient to both linear and nonlinear perturbations.

In contrast, the first excited guided mode ($m = 1$) undergoes a well-defined transition between two distinct dynamical regimes, as shown in Fig. 9b. In the stable region (blue), the linear inter-waveguide coupling efficiently compensates the repulsive nonlinear interaction, thereby preserving the nodal structure and spatial localization of the mode. Outside this domain, in the unstable region (red), the balance between coupling and nonlinearity is disrupted, leading to a progressive deformation of the transverse profile, radiation emission, and eventual relaxation into the fundamental guided state.

For higher-order modes ($m = 2$ and $m = 3$), no dynamically stable regions were identified within the explored parameter space. Nevertheless, the instability dynamics of the $m = 2$ mode reveal two distinct decay pathways, as illustrated in Fig. 9c. At relatively weak coupling strengths, the mode undergoes direct collapse into the fundamental state (red region). As the coupling coefficient κ increases, the enhanced inter-waveguide interaction partially sustains the excited structure, allowing the $m = 2$ mode to decay preferentially into the first excited state ($m = 1$), as indicated by the green region. By contrast, the third-order mode ($m = 3$) exhibits a uniformly unstable behavior across its entire existence domain (see Fig. 9d), undergoing a rapid and catastrophic collapse directly into the ground state. This outcome underscores that the pronounced nodal complexity of the $m = 3$ guided mode renders it intrinsically unstable, precluding any partial stabilization or intermediate decay channels under the present conditions.

4 Conclusion

We have analyzed the formation, localization, and dynamical stability of stationary modes in a system of two linearly coupled nonlinear waveguides with strongly asymmetric nonlinear responses. While one waveguide supports localization through an inhomogeneous Kerr nonlinearity, the partner waveguide, characterized by a homogeneous, potentially self-defocusing nonlinearity, cannot sustain localized states on its own. Our results demonstrate that linear coupling provides an effective mechanism for inducing localization in the otherwise non-confining waveguide, leading to coupled soliton-like guided modes.

Using coupled nonlinear Schrödinger equations and systematic numerical simulations, we identified families of fundamental and higher-order stationary states and mapped their existence and stability regions in the parameter space of coupling strength and nonlinearity. The analysis revealed pronounced mode-dependent existence thresholds, with higher-order modes requiring stronger coupling to counteract nonlinear repulsion and prevent delocalization. We further showed that strong self-defocusing suppresses local peak intensities while promoting broader spatial profiles, resulting in nontrivial power redistribution between the coupled components.

The dynamical stability study uncovered a clear hierarchy of robustness: the fundamental mode remains stable throughout its existence domain, the first excited mode is stable only within a restricted parameter range, and higher-order modes are intrinsically unstable, decaying toward lower-order states through radiation emission and structural fragmentation. These findings highlight the critical role of nodal complexity and coupling-mediated interactions in the nonlinear dynamics of coupled waveguide systems.

Overall, this work establishes coupling-induced localization as a robust mechanism in nonlinear guided systems with repulsive interactions and provides insight into the interplay between nonlinearity, coupling, and stability in complex photonic structures. The results may be relevant to a broad class of nonlinear systems where spatially engineered interactions and inter-component coupling govern the emergence and persistence of localized states.

Author contributions B.M.M. performed the numerical calculations and contributed to the interpretation of the results. W.B.C. participated in the numerical simulations and stability analysis. A.T.A. and W.B.C. conceived and supervised the research and coordinated the analysis. B.M.M. and W.B.C. wrote the main manuscript text. All authors discussed the results, contributed to revisions, and reviewed the final manuscript.

Funding The Article Processing Charge (APC) for the publication of this research was funded by the Coordenação de Aperfeiçoamento de Pessoal de Nível Superior - Brasil (CAPES) (ROR identifier: 00x0ma614). The authors acknowledge financial support of the Brazilian agencies Conselho Nacional de Desenvolvimento Científico e Tecnológico - CNPq (#306105/2022-5, #312173/2022-9, 407469/2021-4), Coordenação de Aperfeiçoamento de Pessoal de Nível Superior - CAPES and Fundação de Amparo à Pesquisa do Estado de Goiás - FAPEG. This work was also performed as part of the Brazilian National Institute of Science and Technology (INCT) for Quantum Information (#465469/2014-0). The Article Processing Charge (APC) for the publication of this research was funded by the Coordenação de Aperfeiçoamento de Pessoal de Nível Superior - Brasil (CAPES).

Data availability No datasets were generated or analysed during the current study.

Declarations

Conflict of interest The authors declare no conflict of interest.

References

Akhmediev, N., Ankiewicz, A.: Solitons: Non-linear Pulses and Beams. Springer, New York (1997)

Borovkova, O.V., Kartashov, Y.V., Torner, L., Malomed, B.A.: Bright solitons from defocusing nonlinearities. Phys. Rev. E **84**, 035602 (2011). https://doi.org/10.1103/PhysRevE.84.035602

Borovkova, O.V., Kartashov, Y.V., Vysloukh, V.A., Lobanov, V.E., Malomed, B.A., Torner, L.: Solitons supported by spatially inhomogeneous nonlinear losses. Opt. Express **20**(3), 2657–67 (2012). (https://opg.optica.org/oe/abstract.cfm?URI=oe-20-3-2657)

Cardoso, W.B.: Alternative split-step method for solving linearly coupled nonlinear Schrödinger equations. Comput. Phys. Commun. **307**, 109414 (2025). (https://www.sciencedirect.com/science/article/pii/S0010465524003370)

Cardoso, W.B., dos Santos, M.C.P.: Inducing localized solutions via interaction in a self-defocusing system with localized pumping. Phys. Lett. A **554**, 130726 (2025)

Cardoso, W.B., Zeng, J., Avelar, A.T., Bazeia, D., Malomed, B.A.: Bright solitons from the nonpolynomial Schrödinger equation with inhomogeneous defocusing nonlinearities. Phys. Rev. E **88**, 025201 (2013). https://doi.org/10.1103/PhysRevE.88.025201 dos Santos, M.C.P., Cardoso, W.B.: Spontaneous symmetry breaking induced by interaction in linearly coupled binary Bose–Einstein condensates. Nonlinear Dyn. **111**(4), 3653–64 (2023). https://doi.org/10.1007/s11071-022-07986-3

dos Santos, M.C.P., Cardoso, W.B.: Spontaneous symmetry breaking induced by nonlinear interaction in a coupler supported by fractional diffraction. Phys. Lett. A **537**, 130311 (2025). (https://www.sciencedirect.com/science/article/pii/S037596012500091X)

dos Santos, M.C.P., Malomed, B.A., Cardoso, W.B.: Solitons supported by a self-defocusing trap in a fractional–diffraction waveguide. Chin. J. Phys. **89**, 1474–82 (2024). (https://www.sciencedirect.com/science/article/pii/S057790732400025X)

dos Santos, M.C.P., Bazeia, D., Avelar, A.T., Cardoso, W.B.: Spontaneous symmetry breaking induced by inhomogeneous nonlinearity in the coupled nonlinear Schrödinger equation. Nonlinear Dyn. **113**(2), 1539–50 (2025). https://doi.org/10.1007/s11071-024-10274-x

Driben, R., Dror, N., Malomed, B.A., Multipoles, M.T.: Vortex multiplets in multidimensional media with inhomogeneous defocusing nonlinearity. New J. Phys. **17**(8), 083043 (2015). https://doi.org/10.1088/1367-2630/17/8/083043

Driben, R., Meier, T., Malomed, B.A.: Creation of vortices by torque in multidimensional media with inhomogeneous defocusing nonlinearity. Sci. Rep. **5**(1), 9420 (2015). https://doi.org/10.1038/srep09420

Hacker, N., Malomed, B.A.: Nonlinear dynamics of wave packets in tunnel-coupled harmonic-oscillator traps. Symmetry **13**(3), 372 (2021)

Kartashov, Y.V., Lobanov, V.E., Malomed, B.A., Torner, L.: Asymmetric solitons and domain walls supported by inhomogeneous defocusing nonlinearity. Opt. Lett. **37**(23), 5000–2 (2012). (https://opg.optica.org/ol/abstract.cfm?URI=ol-37-23-5000)

Kartashov, Y.V., Malomed, B.A., Torner, L.: Unbreakable PT symmetry of solitons supported by inhomogeneous defocusing nonlinearity. Opt. Lett. **39**(19), 5641–4 (2014). (https://opg.optica.org/ol/abstract.cfm?URI=ol-39-19-5641)

Kartashov, Y.V., Malomed, B.A., Vysloukh, V.A., Belić, M.R., Torner, L.: Rotating vortex clusters in media with inhomogeneous defocusing nonlinearity. Opt. Lett. **42**(3), 446–9 (2017). (https://opg.optica.org/ol/abstract.cfm?URI=ol-42-3-446)

Kivshar, Y.S., Agrawal, G.P.: Optical Solitons: From Fibers to Photonic Crystals. Academic Press, Boca Raton (2003). https://doi.org/10.1016/B978-0-12-410590-4.X5000-1

Kono, M., Skoric, M.: Nonlinear Physics of Plasmas. Optical, and Plasma Physics. Springer Series on Atomic, Springer, Berlin (2010). https://doi.org/10.1007/978-3-642-14694-7

Lee, F.C., dos Santos, M.C.P., Avelar, A.T., Cardoso, W.B.: Influence of fourth-order dispersion on the formation of localized states in systems with inhomogeneous defocusing nonlinearity. Chaos, Solitons Fractals **202**, 117629 (2026)

Lobanov, V.E., Borovkova, O.V., Kartashov, Y.V., Malomed, B.A., Torner, L.: Stable bright and vortex solitons in photonic crystal fibers with inhomogeneous defocusing nonlinearity. Opt. Lett. **37**(11), 1799–801 (2012). (https://opg.optica.org/ol/abstract.cfm?URI=ol-37-11-1799)

Pethick, C.J., Smith, H.: Bose–Einstein Condensation in Dilute Gases. Cambridge University Press, Cambrdige (2008). https://doi.org/10.1017/CBO9780511755583

Tian, Q., Wu, L., Zhang, Y., Zhang, J.F.: Vortex solitons in defocusing media with spatially inhomogeneous nonlinearity. Phys. Rev. E **85**, 056603 (2012). https://doi.org/10.1103/PhysRevE.85.056603

Wu, Y., Xie, Q., Zhong, H., Wen, L., Hai, W.: Algebraic bright and vortex solitons in self-defocusing media with spatially inhomogeneous nonlinearity. Phys. Rev. A **87**, 055801 (2013). https://doi.org/10.1103/PhysRevA.87.055801

Xie, Q., Wang, L., Wang, Y., Shen, Z., Fu, J.: Bright solitons in nonlinear media with a self-defocusing double-well nonlinearity. Phys. Rev. E **90**, 063204 (2014). https://doi.org/10.1103/PhysRevE.90.063204

Yang, J.: Nonlinear Waves in Integrable and Nonintegrable Systems. Society for Industrial and Applied Mathematics, Philadelphia (2010). https://doi.org/10.1137/1.9780898719680

Zeng, J., Malomed, B.A.: Bright solitons in defocusing media with spatial modulation of the quintic nonlinearity. Phys. Rev. E **86**, 036607 (2012). https://doi.org/10.1103/PhysRevE.86.036607

Zeng, J., Malomed, B.A.: Localized dark solitons and vortices in defocusing media with spatially inhomogeneous nonlinearity. Phys. Rev. E **95**, 052214 (2017). https://doi.org/10.1103/PhysRevE.95.052214

Zeng, L., Zeng, J.: Modulated solitons, soliton and vortex clusters in purely nonlinear defocusing media. Ann. Phys. **421**, 168284 (2020). (https://www.sciencedirect.com/science/article/pii/S0003491620302189)

Zhong, R.X., Chen, Z.P., Huang, C.Q., Luo, Z.H., Tan, H.S., Malomed, B.A., et al.: Self-trapping under two-dimensional spin–orbit coupling and spatially growing repulsive nonlinearity. Front. Phys. **13**(4), 130311 (2018). https://doi.org/10.1007/s11467-018-0778-y